www.elsevier.com/locate/ijadhadh

Effects of Silane Surface Functionalization on Interfacial Fracture Energy and Durability of Adhesive Bond Between Cement Paste and Epoxy

Jovan Tatar, Christa E. Torrence, John J. Mecholsky, Curtis R. Taylor, H.R. Hamilton

PII: S0143-7496(18)30042-3
DOI: https://doi.org/10.1016/j.ijadhadh.2018.02.009
Reference: JAAD2134

To appear in: *International Journal of Adhesion and Adhesives*

Received date: 19 January 2017
Accepted date: 7 February 2018

Cite this article as: Jovan Tatar, Christa E. Torrence, John J. Mecholsky, Curtis R. Taylor and H.R. Hamilton, Effects of Silane Surface Functionalization on Interfacial Fracture Energy and Durability of Adhesive Bond Between Cement Paste and Epoxy, *International Journal of Adhesion and Adhesives,* https://doi.org/10.1016/j.ijadhadh.2018.02.009

1 EFFECTS OF SILANE SURFACE FUNCTIONALIZATION ON INTERFACIAL FRACTURE ENERGY AND DURABILITY OF ADHESIVE BOND BETWEEN CEMENT PASTE AND EPOXY

Jovan Tatar[1], Christa E. Torrence[2], John J. Mecholsky[3], Jr.Curtis R. Taylor[4], H. R. Hamilton[5]

Abstract

Epoxy adhesives are experiencing widespread use in concrete structures. However, a common concern regarding the adhesive joints in the infrastructure is their durability when exposed to harsh environments, most particularly, high levels of moisture. This work recognizes that adhesive bond between epoxy and substrate resists applied loads by a combination of chemical (hydrogen) bonds and mechanical interlock. Given the complexity of the stress-transfer mechanism this work focused exclusively on the chemical bond component between epoxy and cement paste, while the mechanical interlock was minimized through polishing of the cement paste substrate. A beam adhesion test method with notched interface was developed to assess the durability of chemical bonds between the adherents when aged by water immersion; surface functionalization of cement paste substrate was additionally explored as means of improving the chemical bonding and adhesion along the interface. Test results indicated that interfacial fracture energies were improved in both dry and conditioned groups with silane surface treatment. Analysis of interfacial failure modes with respect to the analytical crack kink criterion revealed that interphase region between epoxy and cement paste is characterized with higher fracture toughness than the cement paste substrate. The study lays groundwork for improvement in the durability of adhesive joints in related infrastructure through bottom-up interface design.

Keywords: epoxy; concrete; silane; adhesion; durability; hygrothermal.

[1] Assistant Professor, University of Louisiana at Lafayette, Department of Civil Engineering, 131 Rex Street Lafayette, LA 70503, phone: +1 337 482 1118, e-mail: jtatar@louisiana.edu

[2] Graduate Student, Texas A&M University, Department of Materials Science and Engineering, 503 CE Office Bldg, 3136 TAMU, College Station, TX 77843, phone: +1 352-551-5130, email: ctorrence@tamu.edu

[3] Professor, University of Florida, Department of Materials Science and Engineering, 172 Weil Hall, Gainesville, FL 32611, phone: +1 352 846 3306, e-mail jmech@mse.ufl.edu

[4] Associate Professor, University of Florida, Department of Mechanical and Aerospace Engineering, 312 Weil Hall, Gainesville, FL 32611, phone: +1 352 392 2177; e-mail: curtis.taylor@ufl.edu

[5] Professor, University of Florida, Department of Civil and Coastal Engineering, 365 Weil Hall, Gainesville, FL 32611, phone:+1 352 392 9537 x1509, e-mail: hrh@ce.ufl.edu

2 . INTRODUCTION

Epoxy adhesive joints are becoming increasingly used in concrete structures. Some examples include strengthening and repair schemes implementing externally bonded fiber reinforced polymer (FRP) composites, near surface mounted (NSM) FRP, adhesive anchors, segmental bridge construction, bonding of new concrete to old, etc. The integrity of bonded joints is dependent on the ability of the adhesive to maintain its adhesion and mechanical properties throughout the service life of the joint. High levels of moisture, in particular, were found to be damaging to both the properties of the adhesive [1], and its adhesion to the concrete substrate [2]. This degradation of bond due to moisture conditioning leads to transition of failure mode from cohesive (failure within the concrete substrate) in unaged joints to interfacial failure along the interface between epoxy and concrete in aged joints.

Adhesives joints in concrete transfer stress by means of two distinct mechanisms [3]: (1) chemical bonding, and (2) mechanical interlock. The first component is a result of chemical interactions between the adhesive and concrete substrate, while the latter one is due to the inherent tortuosity of the concrete substrate surface. The commonly employed epoxy adhesive in civil infrastructure is diglycidyl ether of bisphenol A resin (DGEBA) monomer which is cross-linked with an amine-rich hardener; these epoxies were found to chemically bond to concrete via weak hydrogen bonds which can be disrupted by the presence of water molecules at the interface. This study examines the durability of chemical bonding between epoxy and cement paste (when no mechanical interlock is present), and explores silane functionalization as a method of bottom-up approach to improving the overall interfacial fracture toughness and durability.

3 BACKGROUND

3.1 Effect of Silane Coupling Agents on the Adhesive Bond

Hydrogen bonding between cement paste hydration products and epoxy is thought to be established between nitrogen atoms of the adhesive and hydroxyl groups of the substrate (O−H···:N), and/or between oxygen and hydrogen atoms in the adhesive and substrate (O−H···:O) [4, 5]. The energy required to break these bonds is on the order of 30-50 kJ/mol , which is very small compared to the energy required to break covalent bonds (on the order of 450-700 kJ/mol) [6]. Additionally, due to their polar nature, hydrogen bonds can be easily disrupted by water molecules; this is thought to be a

contributing mechanism to the overall degradation of epoxy-concrete interfaces [7]. On the other hand, the lack of dependence on polarity is thought to make covalent bonds less vulnerable to the effects of aqueous environments.

To improve chemical bonding between epoxy and concrete, a few researchers employed silane coupling agents. Silanes consist of Si molecules that host two types of functional groups, one that can establish covalent bonds with organic materials and the other one that bonds covalently with an inorganic material, which allows it to form covalent bonds between the adhesive and substrate indirectly. Ye et al. [8] used silane treatment to examine its effects on global fracture energy of bonding between CFRP and concrete and found that silane had improved the fracture energy in specimens with improper surface preparation [8]. No significant improvement in bond strength in the samples with properly roughened substrate was reported, likely because the failure mode shifted from interfacial to cohesive (through the concrete substrate). Choi et al. [9] tested the durability of bonding between epoxy and silane-treated concrete to water, using the slant shear test method [9]. The researchers used epoxy-functional silane (3-glycidoxypropyltrimethoxysilane—GPTMS) to functionalize the concrete surface prior to bonding. While the control groups (dry conditions) showed no statistically significant difference between the silane-treated and non-treated cement substrate, the silane-treated group presented better resistance to deleterious effects of water on bond properties. Another study examined the effect of concrete surface functionalization with γ-glyci-doxypropyltrimethoxysilane (γ-GPS) on sub-critical crack growth along the interface between CFRP and concrete in dry and humid environments [10]. The study reported improved resistance to sub-critical crack growth in specimens that were treated with silane.

Stewart et al. [11] examined the change in contact angle and XPS spectra of cement paste surfaces treated with three different silanes: Aminopropyltriethoxy silane (APTES), 3-glycidyloxypropyltrimethoxy silane (GPTMS), and methoxy terminated polydimethxyl siloxane (PDMS) [11]. While APTES decreased the contact angle, an increase was observed in PDMS-treated samples. This observation was explained by the hydrophilicity and hydrophobicity of the free functional groups in respective silanes. GPTMS presented no significant change in contact angle, most likely due to its functional groups not presenting neither hydrophilic nor hydrophobic preference. Deconvolution of the O 1s and Si 2p electron orbitals from XPS spectra showed an increase in bridging Si and O atoms, which is

indicative of the successful formation of covalent bonds between three of the silanes and cement paste. This finding explains the mechanism behind the positive effect of silanes on the durability of adhesive bonds between concrete and epoxy reported in the literature.

3.2 Fracture Criterion for Interfacial Cracks

Energy available for a unit length growth of crack lying at the interface between two adjoined materials is termed *interfacial energy release rate* (G). Once this energy release rate reaches its critical value, termed *interfacial fracture energy* (Γ_i), the conditions have been satisfied for a crack to extend along the interface:

$$G = \Gamma_i \tag{1}$$

In adhesive interfaces fracture energy (Γ_i) has two components [12]: (1) the intrinsic adhesion energy (Γ_0) and (2) an order of magnitude larger component that is due to energy dissipation mechanisms (ζ):

$$\Gamma_i = \Gamma_0 + \zeta \tag{2}$$

In a flat surface without chemical/mechanical pretreatment, the intrinsic adhesion energy was found to be in good agreement with thermodynamic work of adhesion (W_A) [12]; and therefore, it is clearly representative of secondary bonds formed between the adherents. Thermodynamic work of adhesion is defined by the Dupré equation:

$$\Gamma_0 = W_A = \gamma_s + \gamma_a - \gamma_{sa} \tag{3}$$

where γ_s and γ_a are surface free energies of substrate and adhesive, respectively; and γ_{sa} is interfacial free energy between the substrate and adhesive.

In a realistic interface, however, multiple mechanisms would be engaged during crack growth; clean interfacial failure is only possible under special conditions. In surfaces that were subjected to silane treatment and etching, it was found that intrinsic adhesion energy was greater than the corresponding

thermodynamic work of adhesion [12]. They accredited this to a different failure mode that occurred in these samples. In a general case the *intrinsic fracture energy* (Γ_C) can be represented as [13]:

$$\Gamma_C = i\Gamma_i + s\Gamma_s + a\Gamma_a \tag{4}$$

where i, s, and a are area fractions of interfacial failure, substrate failure and cohesive failure of the adhesive, respectively; and Γ_i, Γ_s and Γ_a are respectively interfacial fracture energy, cohesive fracture energy of substrate, and cohesive fracture energy of the adhesive.

The second term in Eq. (2), ζ, is normally orders of magnitude larger than the intrinsic adhesion energy, and is a result of viscoelastic energy dissipation, heat generation, and friction. While mostly dependent on the adhesive material properties, ζ was found to scale with the intrinsic adhesion energy [12], which indicates that both components are important in the total interface fracture energy Γ_i.

4 RESEARCH MOTIVATION

As previously explained, the bond between epoxy and concrete transfers the applied loads through a combination of chemical (hydrogen bonding) and mechanical interlocking mechanisms. While in cohesive failure modes (crack extension through the substrate), energy required to form new surfaces corresponds almost entirely to fracture energy of the substrate or transition region between epoxy and cement paste (interphase), in case of purely interfacial crack growth the total interfacial fracture energy (Γ_i) represents a combination of contributions from chemical bond ($\Gamma_{chemical}$), and bonding surface tortuosity (mechanical bond) ($\Gamma_{mechanical}$) components:

$$\Gamma_i = \Gamma_{chemical} + \Gamma_{mechanical} \tag{5}$$

where $\Gamma_{chemical}$ and $\Gamma_{mechanical}$ are apparent fracture energies that inherently contain both the intrinsic adhesion and dissipated energy components. $\Gamma_{chemical}$ corresponds to a case where no mechanical interlock is present, while $\Gamma_{mechanical}$ is the contribution to Γ_i from the substrate tortuosity effects.

Previous work on the durability of bonding between epoxy and cementitious materials has concentrated on the evaluation of overall change in fracture energy during accelerated conditioning, without considering the effects of harsh environments on each of the two bond components [14, 15, 16]. While the results from tests quantifying an overall effect on bond provide useful information for the design

of epoxy-concrete bonded joints, they do not offer insight into the exact mechanisms behind bond degradation. Moreover, due to the transition of failure mode from concrete substrate failure (cohesive failure mode) in dry ambient conditions to interfacial separation failure mode following moisture conditioning, the understanding of the relative contribution of chemical and mechanical bonding mechanisms is obscure. Work presented here provides characterization of fracture energy associated with chemical bonding primarily ($\Gamma_{total} = \Gamma_{chemical}$), which is accomplished by minimizing the tortuosity of the bonding surface ($\Gamma_{mechanical} \approx 0$) through a vigorous polishing technique. Use of silane coupling agents to functionalize the cement paste surface and improve the chemical bond were also explored. The previous studies on silane functionalization have not examined the effects of silane surface treatment in a case where mechanical bonding is minimized, and therefore, it is difficult to ascertain whether surface tortuosity has an influence on the effectiveness of silane functionalization or not; the presented work addressed this concern. Two main hypotheses were tested:

1. Chemical bond component ($\Gamma_{chemical}$) between cement paste and epoxy is severely degraded when the interface is saturated with water.
2. Silane coupling agent surface treatment can improve the durability of the chemical bond component ($\Gamma_{chemical}$) between epoxy and cement paste.

5 TEST METHOD

For quantification of chemical bonding between epoxy and cement paste, a three-point bending test, shown in Figure 1, was designed. The test specimen consists of two cement paste bars bonded together with epoxy. A notch (precrack) is incorporated into the specimen between epoxy and cement paste to initiate a crack at one of the interfaces. This failure mode, as discussed earlier, allows quantification of the fracture energy associated with the chemical bond component; effects of surface tortuosity on the test results were minimized by polishing with increasingly fine abrasives until the bonding cement paste surface was as smooth as possible.

A three-point bending test setup was selected over a more commonly utilized four-point bending test due to the rigidity of the test fixture of the four-point bending test, and small deflections at fracture load. The main concern with using four-point bending test was that one of the loading points would not come in contact with the test specimen (due to artifacts introduced by imperfections in specimen

preparation, and those in the test fixture) under very low expected deflections at fracture. This artefact would have resulted in changed shape of the moment diagram, and shear loading at the location of the notch. Similar three-point bending test method is used for fracture toughness determination of ceramics (ASTM C1421) [17].

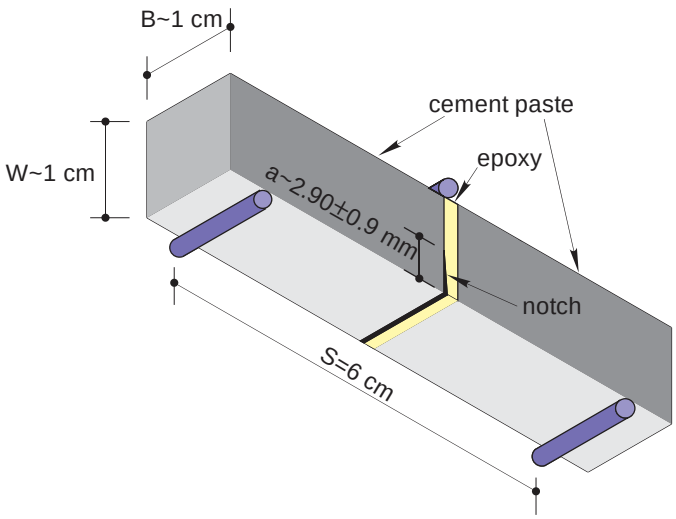

Figure 1. Diagram of three-point bending test used to quantify chemical bonding between epoxy and cement (not to scale).

6 TEST MATRIX AND ACCELERATED CONDITIONING PROTOCOL

Specimens were divided into four test groups, as shown in Table 1. Two control groups were formed: one with silane treatment (S-C), and one without (NS-C); both control groups were held in standard laboratory conditions (23±3˚C, 50±10% R.H.) before testing. The remaining two groups of specimens were also one silane-treated (S-4), and one without silane treatment (NS-4); both groups were conditioned by water immersion at 30ºC for 4 weeks, following one week of curing in standard laboratory conditions. Conditioning time was selected based on the previous moisture diffusion studies that examined times required for epoxy-concrete bondline to reach its moisture equilibrium [18]. Exposure was conducted in tap water in a 34-liter water tank with a circulating pump and a heating element. Composition of tap water is as follows [19]: hardness: approximately 140 mg/L as CaCO3 (8.2 grains/gal); pH: 8.6; sulfate: 97.4 mg/L; chloride: 26.3 mg/L; ammonia: 0.24 mg/L. Water temperature was continuously monitored throughout the exposure with a thermocouple; temperature readings were taken on an Omega HH314A humidity and temperature meter and were in the 30.5±0.2ºC range. All four groups

were tested sequentially on the same day within the first two hours after being removed from the exposure tank.

Table 1. Test matrix.

Group	Surface Treatment	Exposure Condition	Number of Samples
NS-C	None	SLC	8
S-C	Silane	SLC	8
NS-4	None	30ºC water immersion	6
S-4	Silane	30ºC water immersion	7

7 SPECIMEN PREPARATION PROCEDURES

Ordinary Portland cement (OPC) paste cubes (Cemex Type I/II), measuring 5 cm, with a water-to-cement (w/c) ratio of 0.40 were prepared by mixing in a high shear mixer and pouring into brass molds. High shear mixing was chosen over standard paddle mixing to produce a more uniform mixture with low porosity, given that the main goal of the test was to study the chemical bonding between the adherents. Fresh cement paste was covered with a Teflon sheet to minimize moisture loss, and allowed to harden for 24 hours. The cubes were then transferred to a tank with lime solution in tap water for 6 months. Following cure, the samples were stored in standard laboratory conditions for an additional 6 months. Cement paste bars, measuring 5 cm in length and approximately 1x1cm in cross-sectional dimensions, were cut from 10-cm cubes with a low-speed diamond saw (Allied TechCut 4). One end of each bar was then polished to a mirror finish by successive polishing with silicon carbide discs in the grit order 240, 320, 600, 800, 1200, 4000, followed by 2-3 minutes of polishing with 1 um diamond solution in PEG on Buegler TexMet P perforated polishing pad. The resulting root mean square (RMS) roughness of a 50x50 μm area, as determined from Asylum Research MFP-3D atomic force microscope (Figure 2), was between 200-300 nm, which is in the range of intrinsic surface roughness of cement paste [20]. Lower surface roughness cannot be achieved due to the naturally occurring porosity.

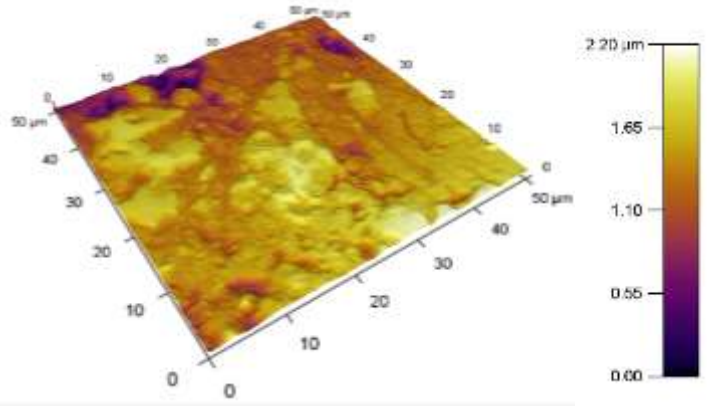

Figure 2. AFM topographic image of a 50x50 µm area of cement paste obtained in intermittent tapping mode on Asylum Research MFP-3D.

8 SILANE SURFACE TREATMENT

Following polishing, all bars were thoroughly cleaned with acetone and randomly separated into two groups: (1) silane-treated; and (2) group without surface treatment. An epoxy-functional silane, 3-glycidoxypropyltrimethoxysilane (GPTMS), was selected for functionalization of silane-treated group. The silane solution was prepared by mixing 1 wt% of the GPTMS in 90:10 wt% ethanol and deionized water solution. A few drops of acetic acid were added to bring the pH of the solution to approximately 5. The mixture was then stirred for 60 minutes in a magnetic stirrer to allow for complete hydrolysis of the silane. The prepared solution was pipetted on the polished surfaces of cement paste bars, and allowed 10 minutes to absorb into the surface before placing the samples in an oven for 80 minutes at 60ºC. This surface functionalization procedure was found to result in the formation of covalent bonds between the silane molecule and cement paste substrate [11].

9 BEAM SPECIMEN PREPARATION

Beam specimen assembly procedures are outlined in Figure 3. PTFE tape was applied to one of the bonding faces of a cement paste bar to prevent adhesion between the epoxy and cement paste at that location and simulate the notch (Figure 3—Step 1). Two cement paste bars were then placed 1 mm apart, and PTFE tape was applied to the sides and bottom of the specimen (Figure 3—Step 2).

An epoxy adhesive consisting of diglycidyl ether of bisphenol A resin (DGEBA, Momentive® EPON 826) and poly(oxypropylene) diamine (POPDA, Hunstman ® Jeffamine D-230) was mixed in a

weight ratio of 100:32.9, which corresponds to the stoichiometric equivalence between the functional groups. The selected epoxy exhibits brittle behavior under standard laboratory conditions.

The 1 mm gap between the two cement paste bars was slowly filled with epoxy using a syringe to ensure no air was trapped (Figure 3—Step 3). A 1-mm gap was chosen as it is on the similar length order of magnitude as the actual adhesive layer thickness in FRP-concrete bonded joints and it also allowed for easy introduction of a notch at the interface in later steps of specimen preparation.

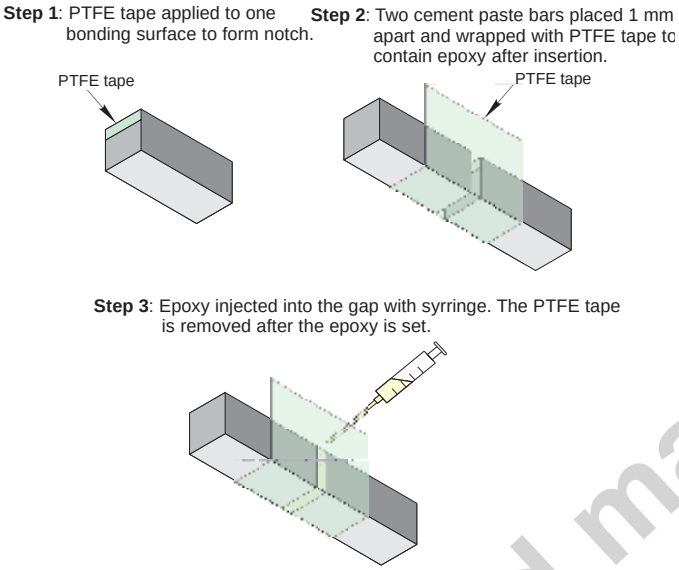

Figure 3. Beam specimen assembly procedures.

To create a sharp notch, following approximately 20 hours of curing in standard laboratory conditions (temperature 23±3ºC and relative humidity 50±10%), the PTFE tape was removed from the interface, and a 0.22 mm thick razor blade was inserted at the interface at a slight angle. Epoxy was cured at standard laboratory conditions for an additional 48 hours before removing the razorblades. The notch created in this manner was additionally sharpened with a 0.10 mm thick razor blade in a sawing motion; to increase the friction and removal of material, razor blades were coated with 6 μm diamond suspension before sawing. Fresh blades were used for each sample to maintain the consistency between the specimens. Scanning electron microscopy (SEM) images of a typical notch resulting from the above-described procedure are shown in Figure 4. The radius of the crack tip at the interface was approximately 1.2 μm (Figure 4c), which is very small compared to the total notch length (1-2 mm) which is deemed sharp for evaluation of interfacial fracture energy. Notch length on each specimen was measured using a

reticle eyepiece on an optical microscope; two measurements (on each face of test specimen) were taken, and the maximum value was used as a notch length *a* (Table 2).

After notching, all specimens were subjected to gradual polishing to 1200 grit to remove the surface flaws (Figure 5). Control beam preparation included coating the cement paste bars (away from the interface) with a thin layer of epoxy to reduce the probability of surface flaws causing undesireable failure in cement paste, away from the notched interface. The exposure group was not coated with epoxy, as an interfacial failure mode was expected due to degradation of the adhesive bonds.

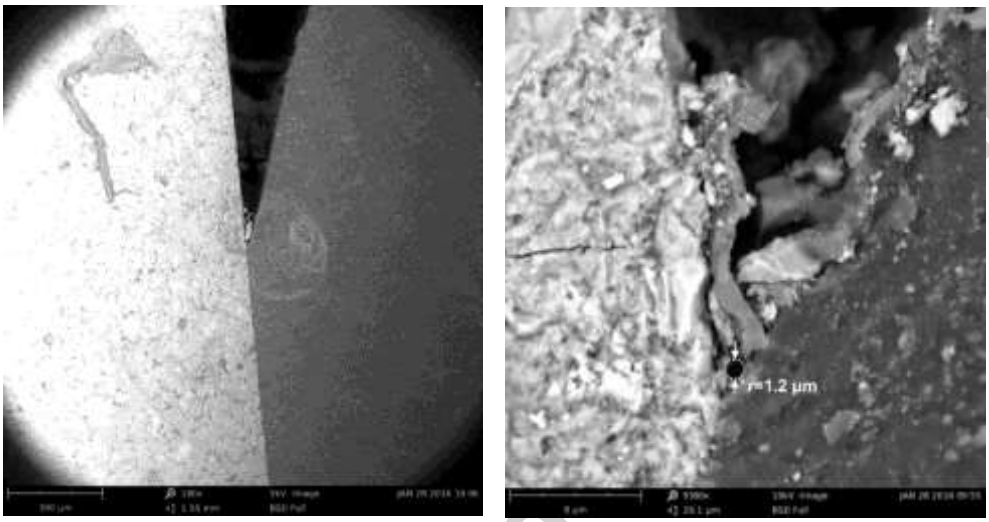

(a) (b)

Figure 4. SEM backscatter image of notch at interface at: (a) 100x; and (b) 9300x.

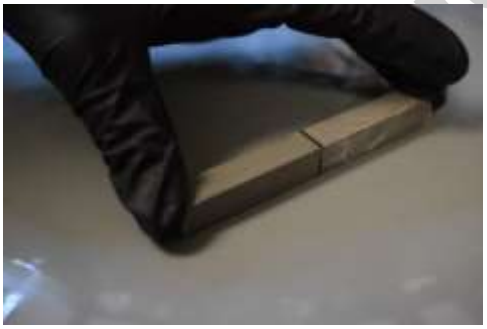

Figure 5. Photograph of polishing of beam specimen.

10 TEST PROCEDURES

All specimens were tested in an Instron universal testing machine (Figure 6). Particular care was taken to align the tip of the loading point with the interfaces. The load was applied at a constant displacement rate of 0.005 mm/sec; data were acquired with a 50-kN load cell affixed to the testing

machine with a noise range of approximately ±0.5 N. Displacement data were collected from the movement of the testing machine cross-head.

Load at fracture and failure mode are reported in Table 2 for all tested specimens. Three typical failure modes were observed: (1) along the notched interface; (2) away from the notch in cement paste; and (3) along the interface opposite from the notch. All conditioned specimens without silane treatment experienced interfacial failure during handling post-exposure without any significant load being applied to them; the assumed failure load of the NS-4 group was, therefore, 0 N for all specimens. Typical load vs. displacement plots are shown in Figure 7; all specimens that achieved the desired failure mode (along the notched interface) experienced unstable crack growth indicating brittle nature of the interface.

Table 2. Summary of test results.

Test Group	Specimen #	Notch Length (mm)	Fracture Load (N)	Failure Location
NS-C	1	2.45	66.09	Notched Interface
	2	3.57	90.71	Notched Interface
	3	2.07	65.11	Notched Interface
	4	4.42	N/A	Notched Interface
	5	1.69	129.68	Opposite Interface
	6	2.82	78.53	Notched Interface
	7	3.14	78.89	Notched Interface
	8	2.63	104.04	Notched Interface
S-C	1	3.58	97.41	Notched Interface
	2	3.39	46.88	Notched Interface
	3	1.96	90.91	Cement Bar
	4	2.45	87.11	Notched Interface
	5	3.86	79.22	Cement Bar
	6	3.01	115.83	Notched Interface
	7	3.86	91.9	Notched Interface
	8	2.11	46.38	Cement Bar
NS-4	1	n/a	0*	Notched Interface
	2	n/a	0*	Notched Interface
	3	n/a	0*	Notched Interface
	4	n/a	0*	Notched Interface
	5	n/a	0*	Notched Interface
	6	n/a	0*	Notched Interface
S-4	1	2.22	45.88	Notched Interface
	2	3.58	27.45	Notched Interface
	3	5.65	12.23	Notched Interface
	4	2.60	20.85	Notched Interface
	5	2.35	26.39	Notched Interface
	6	1.88	28.27	Notched Interface
	7	3.24	17.88	Notched Interface

N/A: the load was not recorded due to loss of connection between testing machine and computer
*: Specimens fractured along notched interface during handling, prior to being tested.

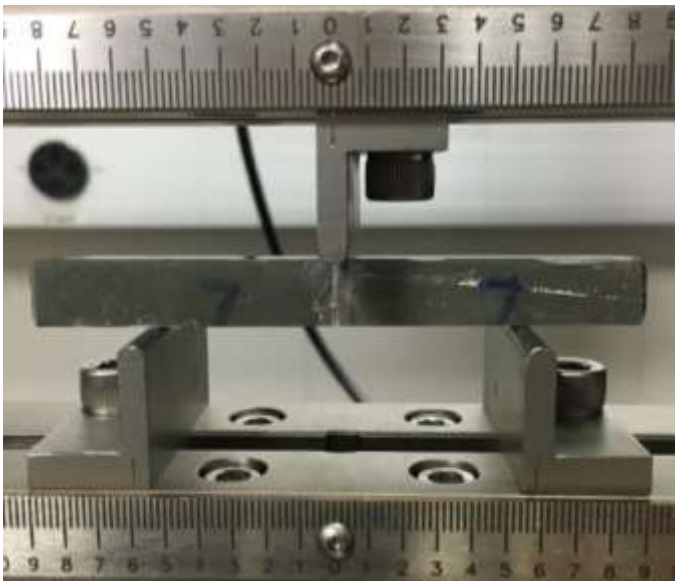

Figure 6. Photograph of beam test specimen in three-point bending fixture.

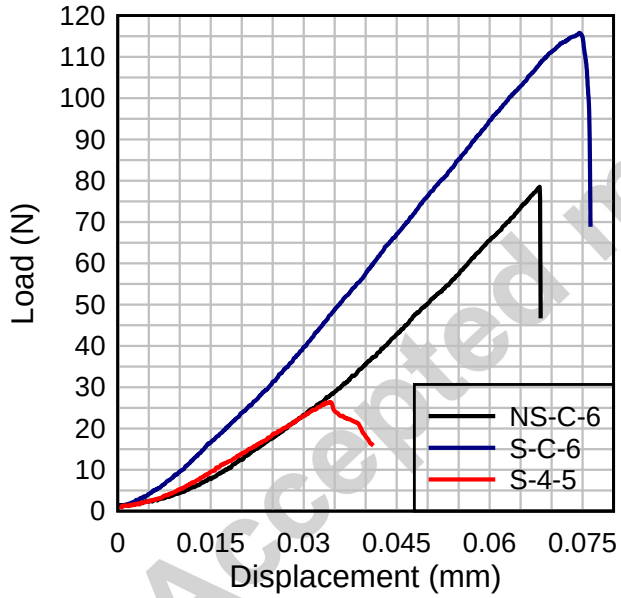

Figure 7. Typical load vs. displacement plots from three-point bending test.

11 DATA ANALYSIS

Data analysis was performed under the framework of interfacial fracture mechanics principles associated with an interfacial crack in a “sandwich”. Considering the principle of energy conservation (J-integral), it can be shown that local (at the crack tip) and global energy release rates are equal [21]. Therefore, there exists a relationship between the local stress intensity factors, and those calculated for a crack in an equivalent homogeneous specimen, when thickness of the adhesive layer is small compared

to all other in-plane dimensions. Interfacial fracture energies were evaluated according to Hutchinson and Suo [21]; the following equation was used:

$$\Gamma_i = \frac{K_{IC}^2}{E^*} \tag{6}$$

where K_{IC} is stress intensity factor at fracture load calculated for an equivalent homogeneous specimen; $E^* = E/(1-\nu^2)$ for plane strain condition and $E^* = E$ for plane stress condition; E and ν are modulus of elasticity and Poisson's ratios of the bulk material (cement paste in this case). Plane strain conditions were assumed in further calculations.

Stress intensity factor in an equivalent homogeneous sample was determined using an equation by Bar-On et al. [22]; the relationship was developed from extensive numerical analyses on cracked beam specimens subjected to three-point bending loading:

$$K_{IC} = \frac{1.5 P_{max} S \alpha^{1/2}}{B W^{3/2} (1-\alpha)^{3/2}} f(\alpha) \tag{7}$$

where P_{max} is maximum load; B and W are respectively width and height of the test specimen; S is span length (6 cm); $\alpha = a/W$ where a is crack length. The value of $f(\alpha)$ is defined by a 5th order polynomial:

$$f(\alpha) = A_0 + A_1\alpha + A_2\alpha^2 + A_3\alpha^3 + A_4\alpha^4 + A_5\alpha^5 \tag{8}$$

where coefficients A_0 through A_5 are constants that are numerically evaluated as a function of S/W ratio [22].

The tabulated values of A_0 through A_5 [22] allow $f(\alpha)$ to be computed for values of S/W of 4, 5, 6, 7, 8, and 10. S/W ratios of the tested specimens were not integers and ranged from 5.45 to 7.02; to account for the variation in S/W ratio, the $f(\alpha)$ values corresponding to the actual S/W ratios of the tested specimens were interpolated by a 3rd order polynomial (Figure 8).

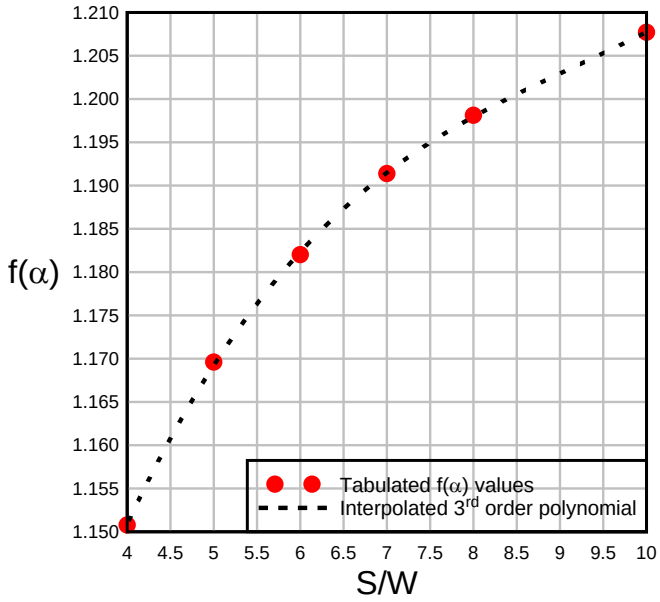

Figure 8. Example of 3rd order polynomial interpolation of $f(\alpha)$.

12 DISCUSSION OF INTERFACIAL FRACTURE ENERGY RESULTS

Interfacial fracture energies corresponding to fracture along the notched interface were calculated for all specimens per Eq. (6); moduli of elasticity for control and conditioned group of 29 GPa and 16.8 GPa were used based on the nanoindentation data [23], respectively. Poisson's ratio of 0.24 for cement paste was used [24]. Results from specimens with other failure modes were not considered. Outliers were identified according to ASTM E178 [25], based on the tabulated values for one-sided 5% significance level. Test results for each test group are summarized in Table 3 and Figure 9.

Table 3. Summary of interfacial fracture energy results.

Test Group	No. of specimens used to compute mean	No. of outliers	Mean±Standard Deviation (J/m^2)	COV
NS-C	6	1	18.9±3.2	0.17
S-C	4	1	31.7±2.0	0.06
NS-4	6	0	0±0	0
S-4	6	1	2.9 ±1.3	0.45

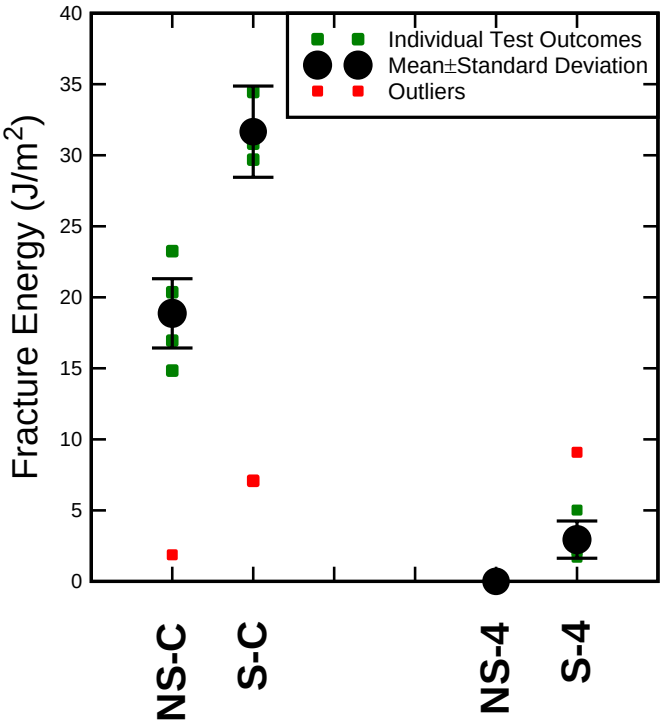

Figure 9. Interfacial fracture energies from three-point bending test on beam specimens.

It is apparent that fracture energies in silane treated samples are higher than those of the corresponding non-treated groups (Figure 9), indicating the effectiveness of surface functionalization on the interfacial fracture energies. While silanes proved to increase the resistance of the adhesive bond to the effects of water, a reduction in fracture energy of 91% from control silane group was noted. This reduction could be due to the low cohesive strength of the deposited layer of the coupling agent combined with the inadequate stability of formed interfacial bonds [26]. Another possibility is that dissimilar chemical interactions occur between silane and different material phases within the cement paste (calcium silicate hydrate, calcium hydroxide, unhydrated clinker, etc.); additional research is required to characterize the interactions between silanes and different material phases in the cement paste under the influence of moisture.

All non-treated conditioned specimens (NS-4) failed during handling while being removed from the conditioning tank. While this is thought to be mostly due to the vulnerability of hydrogen bonds between epoxy and cement paste to the lubricating effect of water molecules at the interface, another potential mechanism that would be disruptive to the integrity of hydrogen bonds was identified: swelling of the adhesive layer. Epoxy adhesives undergo a significant volumetric change due to water sorption,

which introduces stress along the faces of the adhesive that are constrained from free expansion; this behavior was demonstrated in epoxy-cement paste interfaces using photoelasticity test method [23].

Additionally, degradation of mechanical properties of epoxy and cement paste during conditioning would have contributed to an increase in interfacial energy release rate which would result in the specimen failing at a lower applied load [23]. It appears that in NS-4 group the effects of swelling stress, and epoxy and cement paste degradation were significant enough to cause fracture along already degraded interface without the substantial external stimulus.

In the conditioned silane group (S-4), in addition to the possible low cohesive strength of the silane layer and instability of silane bonds, the significant decrease [(91%) from control (S-C)] in fracture toughness can also be attributed to the development of a swelling stress across the interface. The existence of interfacial stress due to swelling of epoxy combined with increased interfacial energy release rate due to deterioration of mechanical properties of epoxy and cement paste [23] indicates that degradation of the interface is a combination of chemical and mechanical phenomena. The test results from the three-point bending test of S-4 group specimens are, therefore, *apparent* interfacial fracture energies; the actual interfacial fracture energies, free of secondary effects due to swelling stress and degradation of the adherents, associated with this group are likely to be significantly higher.

To statistically evaluate the data, the null-hypothesis that means between the two control and two conditioned groups are equal was tested using an unpaired t-test; the main underlying assumption was that interfacial fracture energies in each group were normally distributed. Corresponding P-values are shown in Table 4; for both cases the null-hypothesis was rejected, confirming that statistically significant difference in interfacial fracture energies exists between the non-treated and silane-treated groups, confirming the effectiveness of epoxy-functional silane in increasing the interfacial fracture energy and improving the durability of the adhesive interface.

Table 4. Summary of p-values from unpaired t-test.

Group 1	Group 2	P-value	Reject Null-hypothesis?
NS-C	S-C	0.0002	Yes.
NS-4	S-4	0.0004	Yes.

13 FRACTOGRAPHIC ANALYSES OF FAILED SURFACES

Due to the extremely brittle nature of cement paste, failure in cement paste-epoxy adhesive joints occurs either along the interface between the two materials (interfacial failure mode) or within the cement paste substrate (cohesive failure mode). Failure never occurs cohesively within the epoxy adhesive due to its relatively high fracture energy when compared to the interface and cement paste. The interfacial failure mode is generally associated with deteriorated adhesive interfaces that were subjected to moisture conditioning [2]; such failure modes have not been observed in undegraded adhesive joints which makes quantification of chemical bond fracture energy a challenge.

Following the three-point flexure test, fractured interfaces were examined under optical microscope and SEM to determine the characteristics of the fractured surfaces. Both epoxy and cement paste sides of the failed interface were inspected (Figure 10). Optical microscope photographs of typical failed interfaces in each of the four groups are shown in Figure 11. A special light filter was used to intensify the reflection from the surfaces and exaggerate the contrast between the areas of different roughness: significant yellow light reflection indicates good reflection of light and low surface roughness; while the lack of yellow light reflection is related to relatively high surface roughness. From the reflection of yellow light in images it is apparent that specimens in all groups, except for S-C, have smooth fracture surface which is indicative of the interfacial failure mode. Examination of reflective regions in SEM provided additional evidence that these areas had experienced a clean interfacial failure mode. Secondary electron image (Figure 12a) of cement paste surface shows striations caused by polishing, which signifies that no damage had occurred in the substrate. Similar markings were observed on the epoxy side (Figure 12b), too; same fracture surface features were observed in highly reflective regions (Figure 11) of NS-C, NS-4 (“1a”), and S-4 (“1a”) groups. On the other hand, all control specimens that were treated with silane (S-C group) experienced mostly the cohesive failure mode. Secondary electron and backscatter images taken on cement paste and epoxy side of failed interface (Figure 13a and Figure 13b, respectively), of areas marked with ‘1b’ in Figure 11, show that the crack had bounced between interface and substrate resulting in a rough surface. This is not surprising as it was shown through FEA simulations that for interfaces loaded in Mode I, where interface strength is sufficient, the crack meanders through the weaker material (in this case, cement paste) along the interface [27]. Areas marked with “2b” (Figure 11) mainly experienced interfacial failure mode with some pulled off cement paste grains.

Dark areas on exposed specimens (NS-4 and S-4 test groups), labeled as '2a' in Figure 11, are locations that experienced precipitation of salts (e.g., calcium carbonate) resulting from dissolution of cement paste minerals (e.g., portlandite). As it was confirmed from SEM micrographs (Figure 14)—growth of needle-like crystals was observed which likely corresponds to precipitated calcium carbonate.

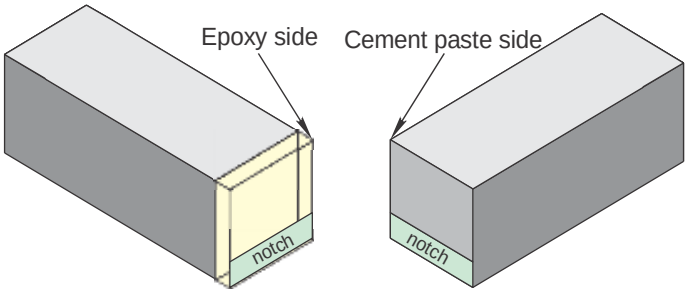

Figure 10. Failed beam specimen. Fracture surfaces on both epoxy and cement paste side of each specimen were examined.

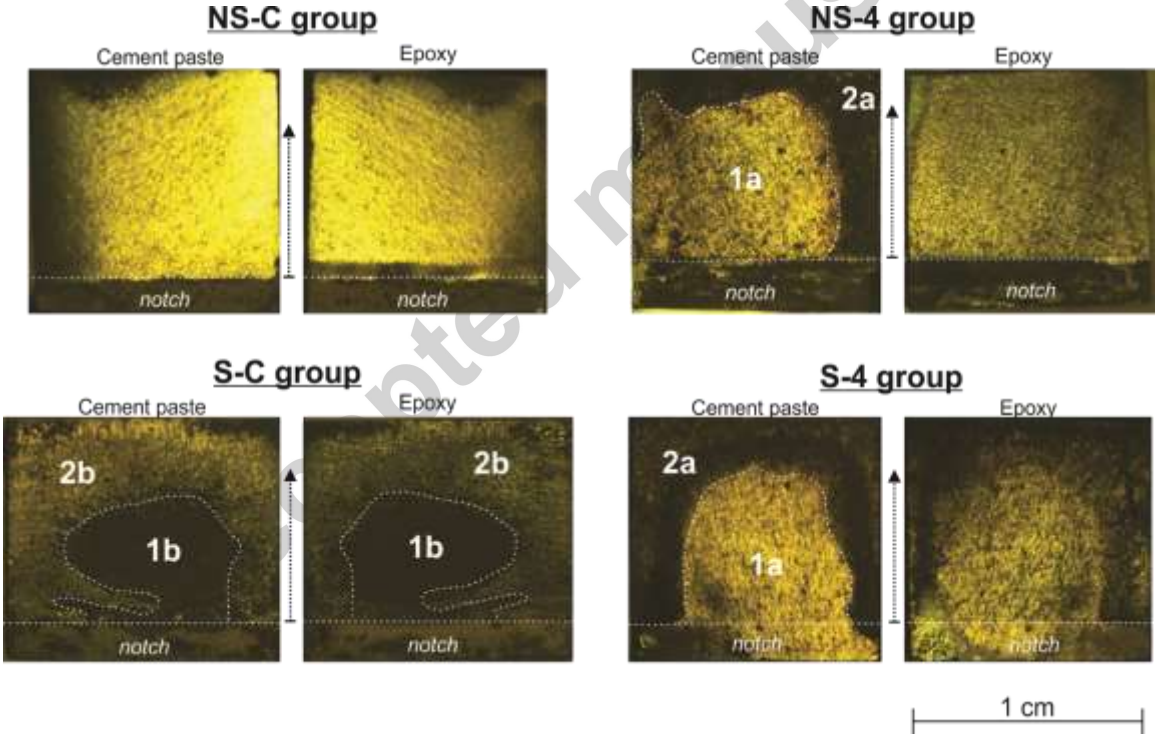

Figure 11. Optical microscope photographs of typical failed interfaces showing cement paste and epoxy adhesive side; arrows signify crack growth direction.

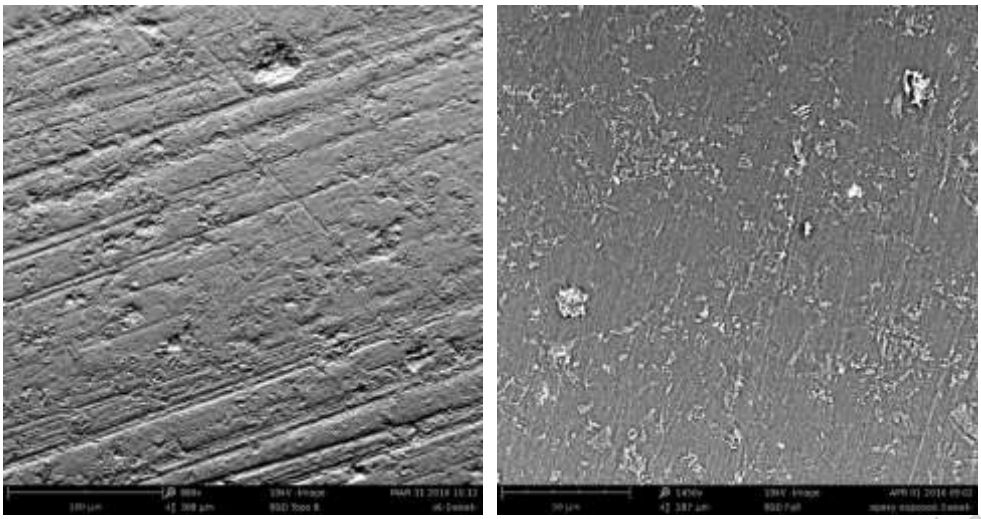

(a) (b)

Figure 12. Typical images corresponding to NS-C, NS-4, and S-4 test groups: (a) Secondary electron image of typical post-mortem cement paste surface showing no damage to the substrate following three-point bending test; (b) backscatter electron image of epoxy surface showing polishing marks with no pulled off cement paste particles (lack of contrast).

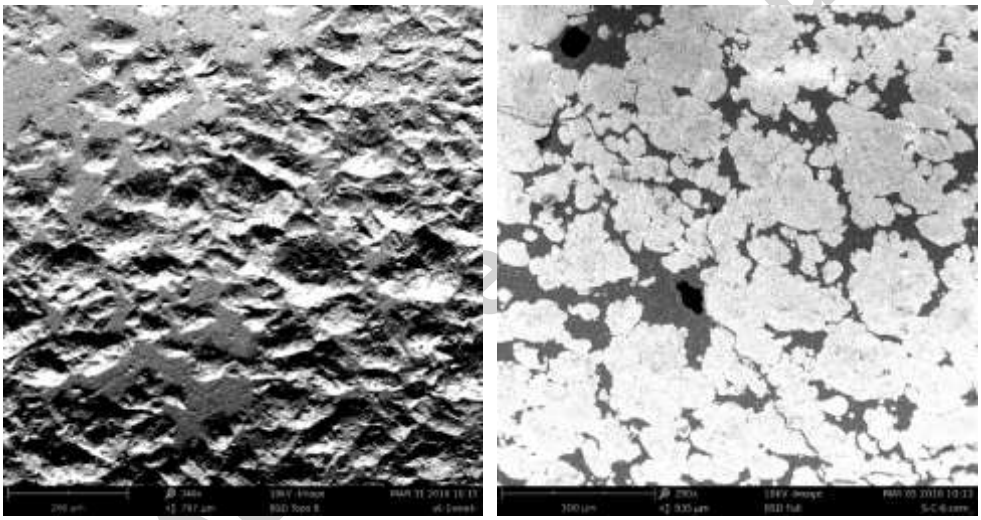

(a) (b)

Figure 13. Images corresponding to S-C group: (a) Secondary electron image of typical post-mortem cement paste surface showing significant changes in topography (smooth and rough regions) indicating mostly cohesive failure mode; (b) backscatter image of typical post-mortem epoxy surface of the interface showing significant changes in contrast (dark areas indicate epoxy surface, and brighter areas correspond to pulled off cement paste grains and cohesive failure mode).

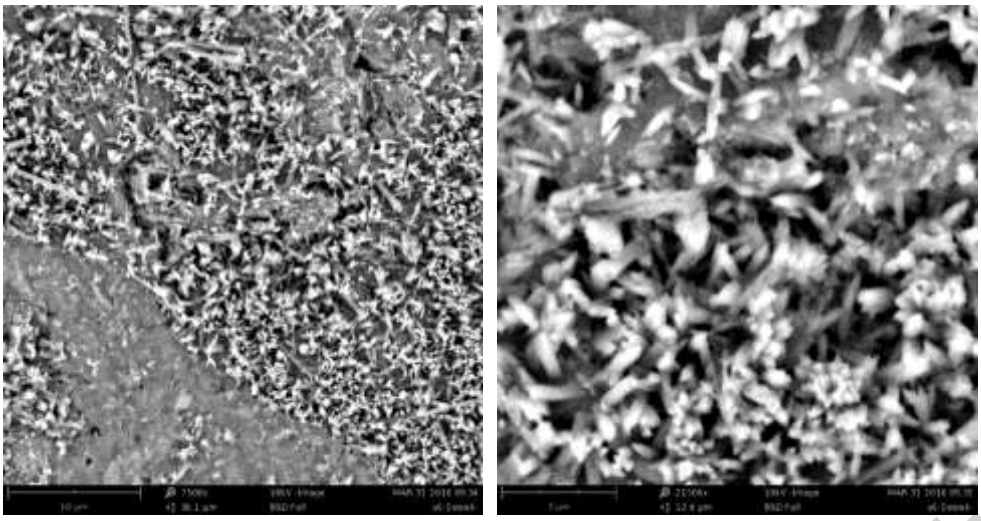

(a) (b)

Figure 14. Precipitated salt crystals on exposed samples at two magnifications (backscatter electron signal): (a) 7500x; and (b) 21500x.

14 EVALUATION OF KINK CRITERION IN RELATIONSHIP TO THE EXPERIMENTAL RESULTS

As it was shown in the previous section, different failure modes were observed between the two control groups (NS-C and S-C). While interfacial failure mode generally indicates that the substrate was tougher than the interface, the opposite is true for a cohesive failure mode. As concrete-epoxy interfaces are to be designed for cohesive failure within the concrete substrate, it is important to evaluate the conditions under which such failure mode is possible.

To further examine the relationship between observed failure modes and measured fracture energies associated with each group of samples, an analytical model considering the kinking of the crack out of a bimaterial interface was considered (Figure 15a). He and Hutchinson demonstrated that a crack will kink out of an interface inside Material 2 when the following criterion is satisfied [28]:

$$\frac{\Gamma_i}{\Gamma_s} \geq \frac{G_i}{G_\omega^{max}} \tag{9}$$

where Γ_i is fracture energy of the interface, Γ_s is fracture energy of the substrate; G_i is energy release rate available for crack growth along the interface; G_ω is energy release rate associated with the kinked crack path inside Material 2; G_ω^{max} represents maximum energy release rate associated with the kinked crack path inside Material 2. When $\Gamma_i/\Gamma_s < G_i/G_\omega^{max}$ crack extends along the interface. The transitioning case is, therefore, $\Gamma_i/\Gamma_s = G_i/G_\omega^{max}$, ω is the kinked crack angle.

Based on He and Hutchinson [28], the crack kink criterion for a bimaterial interface with a significant elastic mismatch (characteristic for epoxy-cement paste interface) is plotted in Figure 15b; mode mixity parameter (ψ) is defined as:

$$\psi = tan^{-1}\left(\frac{K_1}{K_2}\right) \quad (10)$$

where K_1 and K_2 are respectively Mode I and Mode II contributions to the complex interfacial stress intensity factor $K = K_1 + iK_2$. Mode mixity can exist as a result of loading condition, specimen geometry, and elastic mismatch between the adherends.

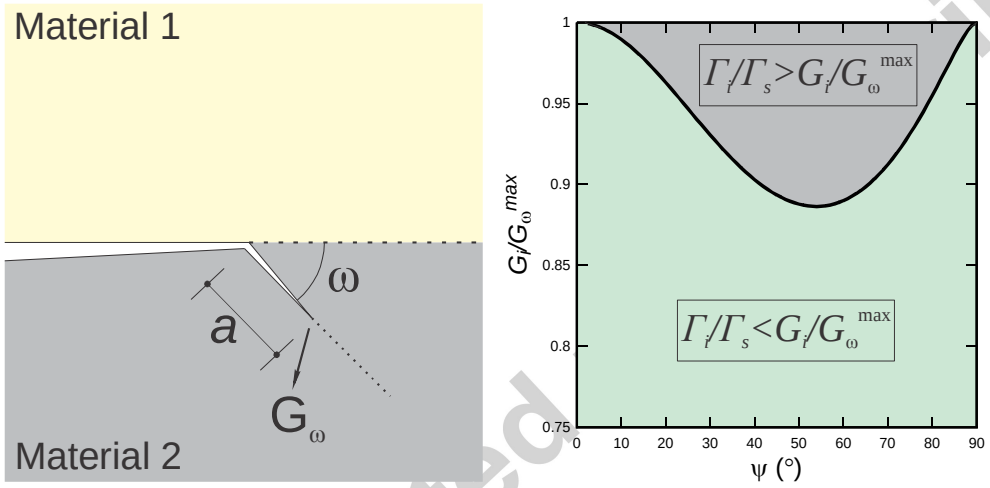

(a) (b)

Figure 15. (a) Graphical representation of crack kinking out of interface (modified from Suo and Hutchinson 1989); and (b) crack kink criterion for epoxy-cement paste bimaterial couple.

In a homogeneous isotropic material, for pure Mode I loading, no mode mixity is present ($\psi = 0°$); however, in this analysis (Figure 15) the entire range of loading modes is considered due to a mode mixity introduced by the mismatch in materials properties, and the those due to imperfections in specimen geometry combined with microscale defects on the surface introduced by polishing. As demonstrated in Figure 15b, to satisfy the crack kink criterion, in the worst-case scenario, Γ_i/Γ_s would have to be greater than 0.88. By comparing the measured interfacial fracture energy of NS-C group (18.87 J/m^2) to those of cement paste found in the literature (Table 5) it becomes apparent that the kink criterion would have been satisfied ($\Gamma_i > \Gamma_s$) which is in conflict with the observed failure mode which

suggests that $\Gamma_i > \Gamma_s$. It should be noted, however, that for a crack to kink out of the interface into the substrate, it would first have to overcome the fracture energy of the *interphase*. Interphase represents a distinct chemo-mechanical transition region between bulk epoxy and bulk cement paste that is a result of permeation of epoxy into the porous structure of cement paste [23]. As shown by Raman spectroscopy and nanoindentation [23], the interphase region can be regarded a composite of cement paste and epoxy, with epoxy occupying some of the porosity. Given that the main fracture-inducing flaws in cement paste are pores (which volume fraction is reduced by permeated epoxy), and also considering the fracture energy of epoxy that is an order of magnitude greater than that of cement paste (Table 5), it can be inferred that the interphase, indeed, is characterized by a greater fracture energy than neat cement paste. Since the S-C group specimens failed within a thin region of the substrate it can be assumed that the measured fracture energies correspond to that of the interphase. Taking the fracture energy corresponding to the S-C group into consideration, when analyzing the kink criterion in reference to the NS-C group, it can be easily shown that $\Gamma_i/\Gamma_s = 18.87/31.66 = 0.60$, which means that kink criterion as defined by eq. (9) is not satisfied in the case of epoxy-interphase interface (Figure 15) for a full range of mode mixities. This is in agreement with the experimentally observed interfacial failure mode in NS-C group.

Considering the crack kink criterion in the S-C- group, from the minimum value in the plot in Figure 15 ($G_i/G_\omega^{max} = 0.88$) and assuming $\Gamma_s = 31.66\, J/m^2$ it can be inferred that the minimum possible interfacial energy release rate of $\Gamma_i = 0.88 \times 31.7 J/m^2 = 27.9 J/m^2$ is associated with the epoxy-cement paste interface, which is still significantly greater than interfacial energy release rate associated with the NS-C group ($18.87 J/m^2$). This demonstrates the significant improvement in interfacial bonding between the epoxy and cement paste following functionalization of the cement paste surface with GPTMS.

Table 5. Cement paste fracture toughness values from literature.

Material	Reference	Fracture Toughness (K_c)	Fracture energy (Γ_c)	Test method
Cement paste	Akono et al. (2011) [29]	$0.66\ MPa\sqrt{m}$	$14.1\ J/m^{2*}$	Micro-scratch test
Cement paste	Higgins and Bailey (1976) [30]	$0.65\ MPa\sqrt{m}$	$13.7\ J/m^{2*}$	Notched three-point bending
Cement paste	Cotterell and Mai (1987) [31]	$0.62\ MPa\sqrt{m}$	$12.5\ J/m^{2*}$	Notched three-point bending test
DGEBA+Jeffamine D-230[a]	Ma et al. (2008) [32]	$0.73\ MPa\sqrt{m}$	$180\ J/m^2$	Compact tension (CT)
DGEBA+Peperidine[b]	Dittanet and Pearson (2012)	$1.11\ MPa\sqrt{m}$	$300\ J/m^2$	Single-edge

	[33]	notch bend (SENB)

*calculated based on elastic modulus from nanoindentation experiments [23]
[a] Huntsman®
[b] Sigma-Aldrich®

15 SUMMARY AND CONCLUSIONS

Mechanical testing was conducted to assess the interfacial fracture energy associated with chemical bonding between epoxy and cement paste in dry conditions, and following conditioning by immersion in 30 ºC water for 4 weeks. Additionally, the influence of substrate functionalization with an epoxy-functional silane (GPTMS) on the interfacial fracture energy associated with chemical bonding, and interface durability was examined. Interfacial fracture energies were measured using an adhesive bond test method that utilizes a beam specimen with a sharp notch in three-point bending to introduce crack growth along the interface. Effects of the mechanical bonding due to the tortuosity of the substrate were minimized by careful polishing of the bonding surfaces.

Test results indicated that chemical bonding in the non-treated group was severely affected by conditioning in water—all conditioned samples failed without any significant external stimulus. This was explained by a combined influence of: (1) hydrogen bond displacement with water molecules; (2) development of swelling stress in the epoxy adjacent to the interface; (3) degradation of the epoxy matrix and cement paste substrate that is deemed to increase interfacial energy release rates, (as shown by Tatar [23]. The silane-treated groups, on the other hand, exhibited a significant improvement in interfacial fracture energy in both control and conditioned groups, when compared to the corresponding dry groups. Conditioned silane-treated samples, however, displayed a degradation of interfacial fracture energy of approximately 91% compared to the control, most likely due to similar effects that occurred in the conditioned non-treated group. Additionally, it is possible that observed degradation in the silane-treated group was also due to the low cohesive strength of the silane layer combined with the instability of bonding between silane and substrate and/or silane and epoxy in an aqueous environment.

Fractographic analyses revealed that all specimens, besides the silane-treated control group, failed along the interface which confirms that the measured interfacial fracture energies were governed by chemical bonding. The silane-treated control group had experienced crack growth within a thin layer of substrate—the measured interfacial fracture energy corresponds to the interphase and represents a lower bound on the fracture energy of the interface. Finally, failure modes were evaluated with respect to the

analytical kink criterion (He and Hutchinson) [28] which indicated that the interphase has a greater fracture energy than neat cement paste substrate.

16 REFERENCES

[1] Blackburn, B.P, Tatar, J., Douglas, E.P., Hamilton, H.R. (2015). "Effects of Hygrothermal Conditioning on Epoxy Adhesives Used in FRP Composites". *Construction and Building Materials*, 96C, pp. 679-689.

[2] Tatar, J., Hamilton, H. R. (2014). "Effect of Moisture on the Adhesive Bond Under Direct Shear". *Proceedings of The 7th International Conference on FRP Composites in Civil Engineering (CICE 2014)*, August 20-22, 2014, Vancouver, Canada.

[3] Tatar, J., Weston, C., Blackburn, P, Hamilton, H. R. (2013). "Direct Shear Adhesive Bond Test", *Proceedings of the 11th International Symposium of Fiber Reinforced Polymer for Reinforced Concrete Structures (FRPRCS-11)*, June 26-28, Guimaraes, Portugal.

[4] Djouani, F., Connan, C., Delamar, M., Chehimi, M. M., Benzarti, K. (2011). "Cement paste-epoxy adhesive interactions". *Construction and Building Materials*, no. 25, pp. 411-423.

[5] Stewart, A. (2012). "Study of Cement-Epoxy Interfaces, Accelerated Testing, and Surface Modification". *PhD Dissertation*, University of Florida, Gainesville, FL.

[6] Callister, W.D., Rethwisch, D.G. (2008), "Atomic Structure and Bonding in Solids", in *Fundamentals of Materials Science and Engineering*, 3rd ed., John Wiley & Sons, Inc., Hoboken, New Jersey, 2008, ch. 2, pp.15-37.

[7] Lefebvre, D. R.; Elliker, P. R.; Takahashi, K. M.; Raju, V. R.; Kaplan, M. L. (2000). "The critical humidity effect in the adhesion of epoxy to glass: role of hydrogen bonding". *Journal of Adhesion Science and Technology*. 2000, 14 (7), pp. 925-937.

[8] Ye, L., Friedrich, K., Weimer, C., Mai, Y. (1998). "Surface treatments and adhesion bonding between concrete and a CFRP composite". *Advanced Composite Materials*, 7(1), pp 47-61.

[9] Choi, S., Maul, S., Hamilton, H.R., Douglas, E. (2013). "Effect of silane coupling agent on the durability of epoxy adhesion for structural strengthening applications". *Journal of Polymer and Engineering Science*, 53(2), pp 283-294.

[10] Amidi, S., Wang, J. (2016). "Subcritical debonding of FRP-to-concrete bonded interface under synergistic effect of load, moisture, and temperature". *Mechanics of Materials*, 92, pp 80-93.

[11] Stewart, A., Scholsser B., Douglas E.P. (2013). “Surface modification of cured cement pastes by silane coupling agents”. *Journal of Applied Materials and Interfaces*, 5(4), pp. 1218-1225.

[12] Andrews, E.H., Kinloch, A.J. (1973a). “Mechanics of adhesive failure. I”, *Proceedings of Royal Society of London A*, 332, pp. 385-399.

[13] Andrews, E.H., Kinloch, A.J. (1973b). “Mechanics of adhesive failure. II”, *Proceedings of Royal Society of London A*, 332, pp. 385-399.

[14] Au, C., Büyüköztürk, O. (2006). “Peel and Shear Fracture Characterization of Debonding in FRP Plated Concrete Affected by Moisture”. *ASCE Journal of Composites for Construction* Vol. 10. No. 1. pp 35-47.

[15] Karbhari, V.M., Engineer, M., Eckell, D. A. (1997). “On the durability of composite rehabilitation schemes for concrete: use of a peel test”. *Journal of Materials Science*, No. 32, pp 147-156.

[16] Tuakta, C., Buyukozturk O. (2010). “Deterioration of FRP/concrete bond system under variable moisture conditions quantified by fracture mechanics”. *Composites Part B: Engineering* 42 (2): 145-154.

[17] ASTM C1421 (2016). “Standard Test Methods for Determination of Fracture Toughness of Advanced Ceramics at Ambient Temperature”. *ASTM International*, West Conhohocken, PA, 2008.

[18] Au, C. (2005). “Moisture Degradation in FRP Bonded Concrete Systems: An Interface Fracture Approach”. Massachusetts Institute of Technology PhD Dissertation, February, 2005

[19] Gainesville Regional Utilities (2016). “Water Chemistry”, https://www.gru.com/OurCommunity/Content/WaterQuality.aspx, accessed on: 01/10/2016.

[20] Trtik, P., Dual, J., Muench, B., Holzer, L. (2008). “Limitations in obtainable surface roughness of hardened cement paste: ‘virtual’ topographic experiment based on focused ion beam nanotomography datasets”. *Journal of Microscopy*, 232(2), pp. 200-206.

[21] Hutchinson, J.W., Suo, Z. (1992). " Mixed Mode Cracking in Layered Materials." *Advances in Applied Mechanics* edited by J. W. Hutchinson and T. Y. Wu, 29, pp. 63-191.

[22] Bar-On, I., Baratta, F.I., Cho, K. (1996). “Crack Stability and its Effect of Fracture Toughness of Hot Pressed Silicon Nitride Beam Specimens”. *Journal of American Ceramic Society*, 79(9), pp. 2300-2308.

[23] Tatar, J. (2016). “Multiscale Analysis of Adhesive Interface between Cement Paste and Epoxy”. *PhD Dissertation*, University of Florida, Gainesville, FL.

[24] Constantinides G., Ulm F.J. (2004). “The effect of two types of C–S–H on the elasticity of cement-based materials: results from nanoindentation and micromechanical modeling”. Cem. Concr. Res. 34, 11, pp. 1293-1309.

[25] ASTM E178 (2008). “Standard Practice for Dealing With Outlying Observations”. *ASTM International*, West Conhohocken, PA, 2008.

[26] Schmidt, R.G., Bell, J.P. (2005). “Epoxy adhesion to metals”. Epoxy Resins and Composites II, Volume 75 of the series *Advances in Polymer Science*, pp. 33-71.

[27] Xuefu, L., Aoki, S. (1992). “Elastic Plastic Crack Growth on Plane Strain Bimaterial Interface”. *Acta Mechanica Sinica*, 8(3), pp. 261-270.

[28] He, M.-Y., Hutchinson, J.W. (1989). “Kinking of a Crack Out of an Interface”. *Journal of Applied Mechanics*, 56(2), pp. 270-278.

[29] Akono, A.-T., Reis, P.M., Ulm, F.-J. (2011). “Scratching as a Fracture Process: From Butter to Steel”. Physical Review Letters, 106(20), 204302.

[30] Higgins, D.D., Bailey, J.E. (1976). “Fracture measurements on cement paste”. *Journal of Materials Science*, 11, pp. 1995-2003.

[31] Cotterell, B., Mai, Y.-W. (1987). “Crack growth resistance curve and size effect in the fracture of cement paste”. *Journal of Materials Science*, 22, pp. 2734-2738.

[32] Ma, J., Mo, M.-S., Du, X.-S., Rosso, P., Freidrich, K., Kuan, H.-C. (2008). “Effect of inorganic nanoparticles on mechanical property, fracture toughness and toughnening mechanism of two epoxy systems”. *Polymer*, 49(16), pp. 3510-3523.

[33] Dittanet, P., Pearson, R.A. (2012). “Effect of silica nanoparticle size on toughening mechanism of filled epoxy”. *Polymer*, 53(9), pp. 1890-1905.